73rd International Astronautical Congress, Paris, France, 18-22 September 2022.

IAC–22–C3.2.1

Towards the commercial development of orbiting reflectors: a technology demonstration roadmap

Andrea Viale* **Onur Çelik, Temitayo Oderinwale, Litesh Sulbhewar, Gilles Bailet, Colin R. McInnes**

Space and Exploration Technology Group, James Watt School of Engineering, University of Glasgow, Glasgow G12 8QQ, Scotland, United Kingdom

Constellations of orbiting solar reflectors on Sun-synchronous repeat ground track orbits can in principle illuminate large terrestrial solar power plants after sunset or before sunrise. This will enhance the number of hours per day during which such solar power plants can deliver clean energy to the grid. In order to develop and deploy such large-scale in-orbit infrastructure, a number of technology demonstrations will be required to de-risk the technology and build confidence for investment. This paper considers potential technology demonstration activities for orbiting solar reflectors, from laboratory-scale testing to high altitude balloon flight and sub-scale in-orbit demonstration. The key technological requirements for orbiting solar reflectors are identified and the utility of each demonstration step evaluated. An integrated technology development, technology demonstration and investment roadmap is then presented.

1. Introduction

Orbiting solar reflectors have long been considered for a range of terrestrial applications, beginning with the work of Oberth in the 1920s [1] through studies in the 1970s [2] and 1980s [3] to recent work by Fraas et al. [4]. A comprehensive review of the concept and discussion of prior studies has recently been published [5]. The key concept considered here is the use of orbiting solar reflectors to illuminate large terrestrial solar power plants. Clearly, the delivery of global clean energy services is an important challenge for the 21st century. With a rapid expansion of the solar energy sector anticipated, orbiting solar reflectors can enhance the utility of solar power farms, in particular when consumer demand is high but output is low. Recent studies have shown that a constellation of reflectors orbiting at an altitude of 1000 km, with an equivalent diameter of 1 km, can deliver up to 36 MWh of energy per pass over a large solar power plant [6]. Other studies have investigated the trade-off between orbiting solar reflectors and battery storage to shunt solar power output after sunset [7]. However, before the concept can reach full-scale commercial deployment, intermediate steps are required to increase its technology readiness level, thus derisking the technology and building confidence for investment.

In this paper a technology demonstration roadmap will be developed. First, a set of requirements for orbiting solar reflectors will be defined including the reflector length-scale, mass properties, slew rates and surface flatness. These are based on the full-scale reference architecture discussed in Ref. [8] Then, laboratory-scale demonstrations will be considered to validate critical technologies, such as scaled structural models for load and vibration testing. Analysis of reflector attitude control strategies can be performed with scaled structural models using an air-bearing facility. Other reflector properties such as membrane wrinkling can also be investigated experimentally.

The use of high-altitude balloons will firstly be considered as a low cost demonstration option. Model verification through such test campaigns will be key to reduce the risk of scaling up the reflector technology to a full-scale commercial constellation. The next step will consider the deployment of a small-scale reflector from a sounding rocket at dawn or dusk, again to illuminate an instrumented test range. A trade-off of sounding rocket apogee, reflector size and pointing requirements will be presented. It is expected that reaction wheels would be used to rapidly slew the reflector and maintain pointing during the short period of free-fall descent. This would allow direct

*Corresponding author
Email addresses:
andreaviale@protonmail.com (A. Viale),
Onur.Celik@glasgow.ac.uk (O. Çelik),
Temitayo.Oderinwale@glasgow.ac.uk (T. Oderinwale),
Litesh.Sulbhewar@glasgow.ac.uk (L. Sulbhewar),
Gilles.Bailet@glasgow.ac.uk (G. Bailet),
Colin.McInnes@glasgow.ac.uk (C.R. McInnes)

Table 1: Requirements table and technology demonstration phase: Laboratory scale demonstration (LD), balloon demonstration (BD), sounding rocket demonstration (SRD) and in-orbit demonstration (OD)

	Req #	Description	LD	BD	SRD	OD
Control requirements	RC1	Control Moment gyros must supply a peak torque of 1704 Nm	✓			
	RC2	Rotation rates below $7.9 \times 10^{-3}\,\mathrm{rad\,s^{-1}}$ (in-plane axis) and $5.1 \times 10^{-3}\,\mathrm{rad\,s^{-1}}$ (normal axis)	✓	✓	✓	✓
	RC3	Actuator mass to reflector mass must be at most 0.6	✓			
	RC4	The centre of the reflected light must cover 90% of the SPF area when overhead				✓
	RC5	Actuator mass density must be $5\,\mathrm{g\,m^{-2}}$	✓			
	RC6	Maximum control moment gyro gimbal rate is 0.4 deg/s	✓			
	RC7	CMG rotor has a diameter of 6.5 m	✓			
Structure requirements	RS1	Structure must withstand critical loads	✓			
	RS2	Structure mass density $< 10\ \mathrm{g/m^2}$	✓			
	RS3	Energy transfer efficiency $> 90\%$	✓	✓		✓
	RS4	Shape distortion due to relative thermal expansion between structure and membrane should be a minimum.	✓			
Manufacturing requirements	RM1	Structure must be manufactured in vacuum	✓			
	RM2	Manufacturing time must be 1% of the lifetime	✓			
	RM3	System must withstand space environment over operational lifetime	✓			✓

measurement of the intensity of reflected light from space to the ground and again verify of the accuracy of numerical models used in the design phase.

An in-orbit demonstration will then be considered by deploying a reflector at an altitude below the International Space Station (for debris mitigation through air drag). This will allow a full end-to-end test of deployment, operation and attitude control of the reflector to reflect sunlight to different Earth sites for measurement of reflected light intensity. Moreover, in-orbit fabrication of the reflector will be considered as a demonstration of full-scale manufacturing of a commercial constellation of reflectors. Finally, the paper will detail the specific requirements and expected outcomes for each demonstration phase. From this analysis an integrated technology demonstration roadmap will be presented, along with the expected timescale for technology development and the investment profile required to lead to the full-scale commercial operation.

2. Technology demonstration steps

Table 1 shows a set of key requirements for testing orbiting solar reflector technology, divided into control, structural and manufacturing requirements. These requirements are based on a full-scale reference architecture study discussed in Ref. [8], where a constellation of five hexagonal reflectors with a side of 250 m is proposed (Fig. 1 shows a representation of one hexagonal reflector). The reflectors are orbiting on a Sun-synchronous repeating ground track orbit at an altitude of approximately 884 kilometers, servicing eight solar power farms with 14 passes every 24 hours. The reflectors are assumed to be fabricated in-orbit from triangular elements. An assembly of four 6.5 m radius control moment gyros (CMGs) are mounted on the back of the reflector, providing a peak torque of 1704 N m.

In the following sections, key technology demonstration tests based on the requirements in Table 1 will then be discussed.

2.1 Laboratory-scale demonstration

The objectives of this demonstration include:

- Validate manufacturing/assembly strategy in the laboratory.
- Qualify structural elements.
- Quantify achievable flatness and reflectivity of the thin film.

The thin metallic film is the payload for the reflector structure, with tensioning ropes required to keep

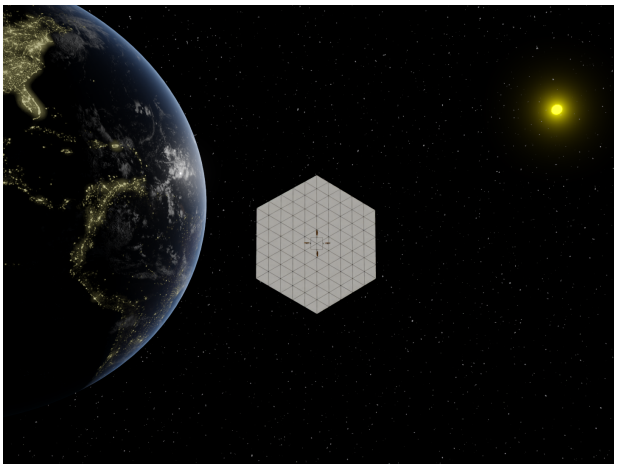

Fig. 1: Representation of an hexagonal orbiting solar reflector in Sun-synchronous orbit (not to scale), discussed in Reference [9].

it acceptably flat. The support structure gives the membrane mechanical strength and withstands the various loadings. The mission demands the following structural requirements:

1. The structure should have enough strength to withstand external and internal loads. The structural arrangement should provide this strength with the minimum possible weight of the structure. These are tabulated in the requirements as RS1 and RS2, respectively.

2. The membrane should be flat enough to reflect the incident light without loss due to wrinking or slackness. This requirement is tabulated as RS3 in the requirements table. To ensure acceptable flatness, the area of the reflector should be maintained in a tensioned state.

3. The distortion due to thermal expansion of the support structure and membrane should be within acceptable limits. This can be accomplished by limiting the difference between the thermal coefficients of structural elements to a minimum possible value, which is enforced as a requirement RS4 in Table 1. Also, the thermal stresses developed should not affect structural integrity.

4. In-Space Addidive Manufacturing is proposed as a manufacturing method for the reflector structure. The manufacturing speed should be able to meet the stipulated timeline of the project. The manufactured parts should meet the required quality standards. These are tabulated as requirements RM in the Table 1.

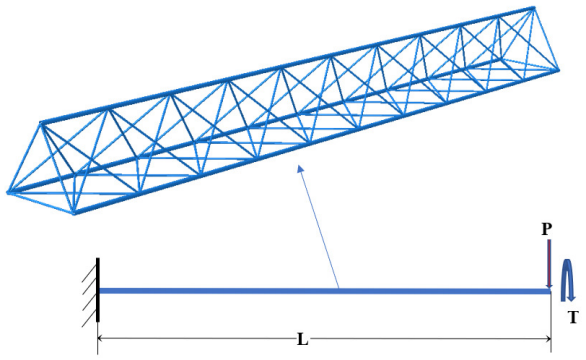

Fig. 2: Bending and torsional strength estimation of a truss beam.

These requirements are now discussed in detail along with the tests required to quantify them.

2.1.1 Structural strength and mass

The support structure is the main load bearing member. A tubular truss type structure is favoured due to its advantages, such as low mass and high strength [10]. The cross-section of the present truss structure is with tubes at the vertices of an equilateral triangle. The reflector is subjected to solar pressure, aerodynamic drag, gravity gradient, control loads and self-rotation forces during its work cycle. From mission analysis, it was determined that the most critical loads are control loads. The maximum control moments exerted on the support structure are known *a priori*. From Ref. [8] the maximum torque generated by the control moment gyros is equal to 1704 N m for the proposed reference architecture. These can be used to calculate the required strength values, which in turn will be used to provide the cross section of the truss.

The equivalent strength of truss beams in bending and in torsion can be determined by laboratory experiments. The cantilever truss beam will be subjected to end loads and torque to estimate the bending stiffness (EI) and torsional stiffness (GJ), as shown in the Fig. 2. E denotes the modulus of elasticity, G the shear modulus, I the second moment of inertia, and J the polar moment of inertia. The results for the laboratory scale specimen can be scaled to the actual size using the bending equation and the torsion equation.

The expression for the deflection of a cantilever

beam subjected to an end load is given as: [11]:

$$\delta = \frac{PL^3}{3EI} \tag{1}$$

Using the above relation, the bending strength can be determined as:

$$EI = \left(\frac{L^3}{3}\right)\left(\frac{P}{\delta}\right) \tag{2}$$

As length is constant, the bending stiffness can be derived using the slope of the relationship between load P and end deflection δ.

Similarly, the torsional strength GJ is determined using the relationship between the angle of twist ϕ and the applied torque T for a cantilever beam as [11]:

$$GJ = L\left(\frac{T}{\phi}\right) \tag{3}$$

Thus, the structural strength requirement outlined using RS1 in the Table 1 is quantified. The limit on the mass of the truss structure stated as requirement RS2 in the Table 1 can be met by using an optimised design for the truss beams and high-strength lightweight composites.

2.1.2 Flatness

An optimum reflector would be a perfectly flat, highly reflective mirror. Deviation from this ideal flat condition is caused by lateral-load-induced curvature and local surface irregularities such as wrinkling. This will lead to diffuse reflectivity, which in turn will cause dispersion of the reflected light.

The relationship between the curvature and the intensity of dispersed light can be derived from energy lost due to dispersion and the curvature of the membrane. The reflected light can be sensed for the different values of the input curvature shown in Fig. 3. If we allow the energy losses up to a certain fraction of the total incident energy, the requirements for the flatness can be derived. These requirements will be input for the tension required to maintain the required flatness. In this technology demonstration, a maximum of 10% energy loss due to deviation in flatness is allowed, stated as requirement RS3 in the Table 1.

2.1.3 Tensioning

Tensioning the membrane is one of the most efficient ways to maintain the desired flatness of a given membrane and to produce a wrinkle-free surface. Testing in the lab will determine both the required tension as well as the margin of operation and

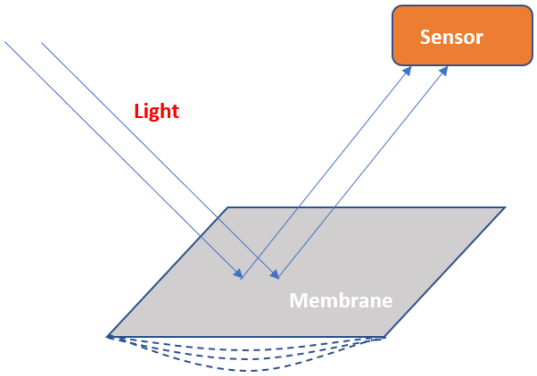

Fig. 3: An experimental concept to estimate the effect of flatness on the intensity of the reflected light.

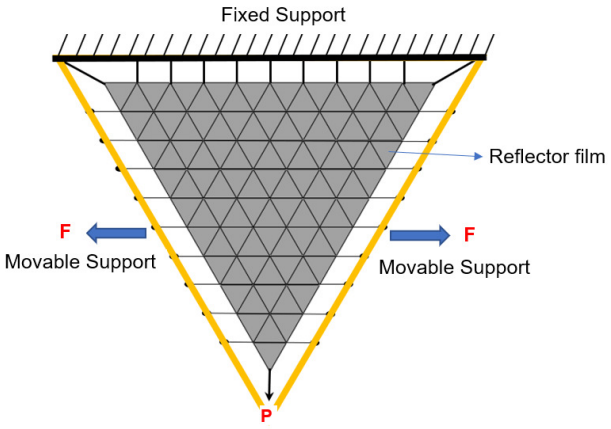

Fig. 4: Estimation of the required tensioning in the membrane.

fatigue limitations to avoid membrane ripping. The reflector for the reference architecture configuration [8] employs triangular shaped reflectors with a triangular tensioning mesh. A scaled sample of membrane is subjected to tensioning with the help of moving and fixed frames as shown in the Fig. 4. A LIDAR (light detection and ranging) based 3D scanner will be used to dynamically monitor the shape of the membrane and deduce the relationship between its curvature and the applied tensioning force. It is to be noted that the force P is equal to the value of tension in each of the ropes to ensure uniform tension. A sensitivity analysis for different sizes of scaled membrane will be used to predict the behaviour of the actual sized reflector.

2.1.4 Thermal expansion

When the reflector is subjected to a temperature field, its shape will change due to the relative thermal expansion of the constituting members. This in turn will affect the flatness of the reflecting membrane. This shape distortion due to the thermal environment should be within acceptable limits according to margins defined in Section 2.1.2.

For the present design of the reflector [8], three elements prone to thermal expansion are particularly susceptible to affecting the functionality of the reflector. The membrane itself, tensioning ropes, and the support structure. The difference between the thermal expansion coefficients of these members should be a minimum to minimise the differential thermal expansion. This is stated as requirement RS4 in Table 1. All those elements can be experimentally tested using infrared lamps (reproducing solar radiative flux) to validate numerical simulations with experimental data. Both small and full scale tests will be conducted, and photogrammetric measurements in conjunction with LIDAR scanners will be used to track dimensional and topological changes. The results obtained over the range of expected in-orbit temperature conditions can be correlated to predict the actual behaviour of the system in space.

Apart from this, the thermal expansion behaviour of the beam truss needs to be evaluated as it is constructed from tubes of various lengths at different orientations, as shown in the Fig. 2. This will lead to thermally induced relative deformations in the support structure. Optical interferometry and strain-gauge methods can be employed for the purpose of measurement of its thermal coefficient of expansion and developed stresses. The developed stresses should be within the limits stated in the strength requirement RS1.

2.1.5 In-Space Addidive Manufacturing

In-Space Addidive Manufacturing (ISAM) is proposed as the main strategy to produce in-orbit the proposed reflectors. Centered around 3D printed units, the ISAM strategy will allow to use several printing end effectors to match the expected manufacturing phase. A test campaign within a cryostat will allow us to precisely take into account the thermal environment of the orbit in the manufacturing time while monitoring manufacturing defects and time associated with repair and qualification of the produced elements. Microgravity tests of the ISAM units will not be necessary for this purpose as previous research has proved that microgravity does not affect 3D printing based on the fused filament fabrication (FFF) process[12].

Once each elements is fabricated, they will be joined by the additive manufacturing. The speed and quality of the joining process can be evaluated to ensure the safety of the structure. This will also validate the assembly time for the reflector's structure.

2.1.6 Actuator testing

The control system requires large scale CMGs. According to RC7, each CMG will be 6.5 meter in diameter and made out of carbon fiber (to increase stiffness and reduce mass of the spokes). Based on RC1, the CMG rotor has a rotational speed of $351.5\,\mathrm{rad\,s^{-1}}$. Those requirements will present a major challenge but an opportunity to demonstrate a new class of control technology able to point accurately extremely large structures with agility with a peak torque of 1704 Nm. In order to test those CMGs, it is important to understand the fact that they are not designed to withstand their own weight. For the laboratory test, we intend to demonstrate the CMGs full scale. For that purpose, one CMG will be tested in an enclosed room able to withstand damage and equipped with remote controls/surveillance. Supports with quick release will be located under the CMG to sustain its weight when not in operation.

At the start of the test, the CMG will be released from its supports and rotate to its maximum rotational speed. A set of cameras will be located within the room to monitor the test and use photogrammetric reconstruction to ensure that the CMG does not deform out of specifications during operations and that the radial and circumferential vibration modes are in line with predictions.

Once this first step is validated, the cage of the CMG will be rotated with a speed of $0.4\,\mathrm{deg/s}$ following requirement RC6. This step will validate both the dynamic behavior of the CMG using the same photogrammetric methodology and provide torque measurement using a load cell equipped with a multiple-bending beam load cells configuration.

Validating the CMG in the laboratory will ensure a conservative qualification of the hardware part of the control system. Full control system validation and qualification will necessitate in-orbit demonstration as described in subsection 2.5.

2.2 Balloon demonstration

The objectives of this demonstration include:

- Power up a light source on the ground using energy received from the reflector.

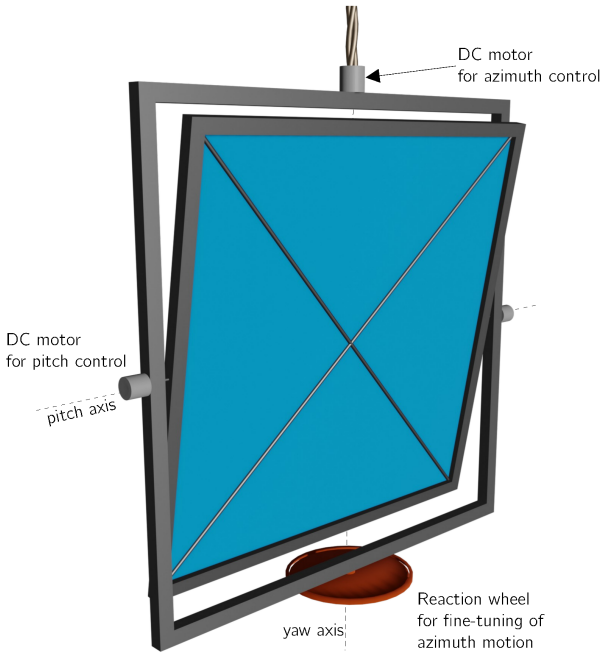

Fig. 5: Reflector attached to balloon gondola.

- Validation of the analytical models discussed in Ref. [9] related power received on the ground.
- Understanding the efficiency of light reflection at lower elevations.
- Validate the models for atmospheric losses.

The main advantage of an air balloon demonstration over other types of static demonstration (for example, sunlight reflection using a mirror mounted in a high altitude spot, e.g., a mountain) is that the the light image on the ground (and therefore the received power density) changes as a function of the elevation, thus validating the analytical model discussed in Refs. [6, 8]. For this experiment, a square reflector is attached to the balloon gondola as shown in Fig. 5. Similar to the design proposed in Ref. [13], the gondola is equipped with two DC motors that enable pitch and yaw rotation. Furthermore, a reaction wheel is used for fine-tuning of the yaw motion.

In order to estimate the power density on the ground, a first approximation model of the balloon trajectory is made. In particular, the balloon is assumed to ascend through the atmosphere with constant vertical velocity and it is assumed that the wind velocity is constant in magnitude and direction. The first assumption is fairly reasonable based on flight data of previous balloon experiments such as BEXUS,

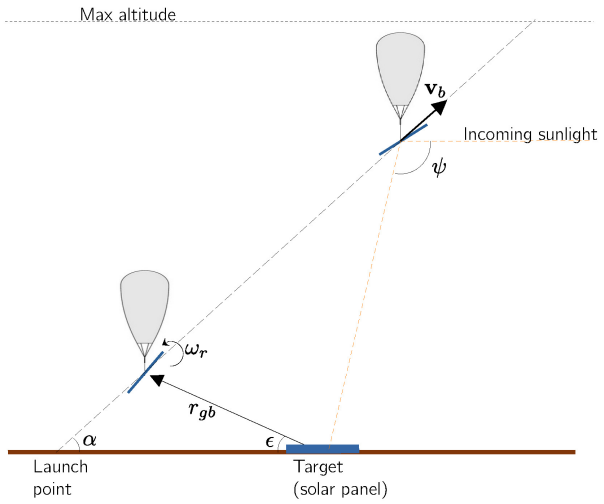

Fig. 6: Air balloon demonstration concept.

whereas the validity of the second assumption clearly depends on local weather conditions.

The horizontal and vertical components of the balloon velocity are estimated using the BEXUS handbook [14]. The horizontal component is assumed to be fixed at $4\,\mathrm{m\,s^{-1}}$, whereas the ascent velocity is $5\,\mathrm{m\,s^{-1}}$. The variation of wind speed direction is neglected here for simplicity, such that the azimuth angle is assumed constant. It is here assumed that the target is positioned on the ground such that at half the ascent time the elevation ϵ of the balloon is 90°.

By inspection of Fig. 6 it can be easily shown that the pitch angle can be written as a function of time as:

$$\psi = \arccos\left(\frac{r_t - v_b t\cos\alpha}{r_{gb}}\right) \tag{4}$$

where r_{gb} is the slant range:

$$r_{gb} = \sqrt{(v_b t)^2 + r_g^2 - 2v_b t r_g \cos\alpha} \tag{5}$$

the angle α is the angle between the velocity vector and the ground, r_g is the distance between the reflector at $t = 0$ and the target. The maximum altitude for a BEXUS flight is between 25 and 30 km. Taking a maximum altitude 27.5 km yields a total ascent time of 1.5 h and a maximum elevation angle of 112 deg. Then, the power on the ground can be expressed as [6]:

$$P = \eta\chi I_0 \frac{A_r}{A_{im}} A_t \cos\frac{\psi}{2} \tag{6}$$

where I_0 is the solar constant, χ is a coefficient describing the transmission efficiency of solar radiation

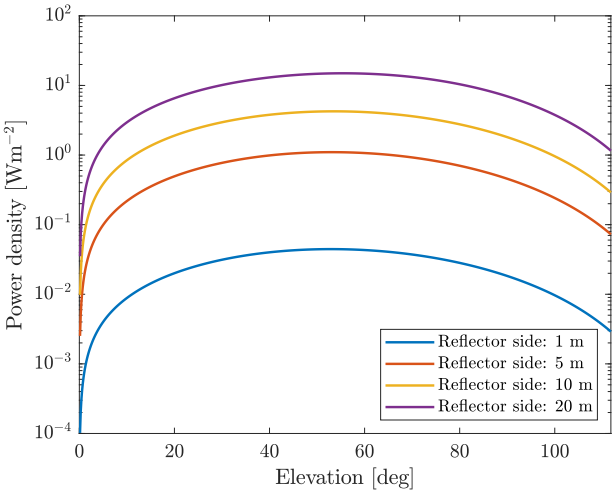

Fig. 7: Variation of power density as a function of time and reflector size, for air balloon demo.

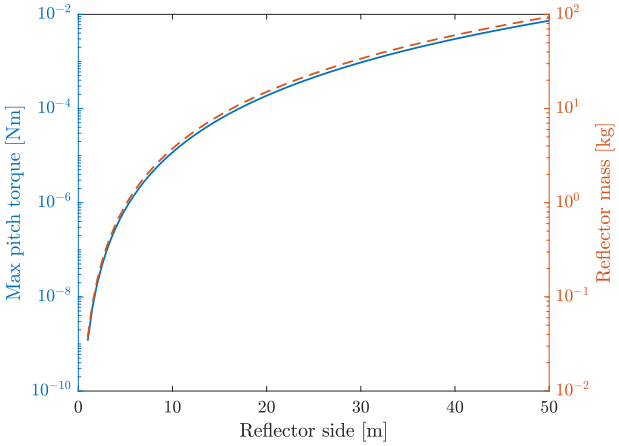

Fig. 8: Maximum pitch motor torque and reflector mass (assuming 37.6 g m^{-2} areal density) as a function of the reflector size.

through an atmosphere that is free of clouds, η denotes the reflectivity, A_r is the area of the reflector, A_{im} is the area of the image on the ground and A_t is the area of the target. The value of A_{im} as a function of the slant range and the reflector size can be found in Ref. [6]. In general, the image area is larger at larger slant ranges. Regarding the transmission coefficient χ, this is a function of the Sun elevation [6] and therefore it depends on the time of the day when the experiment is conducted. In this case, it is expected that the demonstration will occur during dawn or dusk, when the sun has very low elevation. Based on Fig. 5 in Ref. [6], an arbitrarily low transmission coefficient of $\chi = 0.3$ is here selected, corresponding to a Sun elevation of approximately 20 deg. Note that this value will change as a function of time, depending on the exact reflector altitude and the Sun elevation. However, for simplicity, it is considered constant in the following calculations. Based on Ref. [6], the reflectivity coefficient is set to 0.93 in this paper.

Figure 7 shows the power density P/A_t as a function of the elevation ϵ and the reflector size. The peak power density is reached for elevation angles between 55 deg and 60 deg for the reflector side range considered here. Note that, contrarily to the orbit case where the angle ψ is approximately constant [6] and the peak power density is reached when the reflector is overhead (i.e., 90 deg elevation), here ψ is smaller at lower elevation, thus allowing more sunlight to be intercepted, resulting in larger power densities at lower elevations.

Figure 8 shows the required pitch motor torque and reflector mass as a function of the reflector size. The pitch motor torque is estimated with $T = I\ddot{\psi}$, where $I = \sigma_r l^4/12$ is the in-plane inertia of the reflector. Also, a 37.6 g m^{-2} reflector areal density is assumed, which is two times the nominal areal density for the full scale reflector proposed in Ref. [8]. Required torques are below 1×10^{-2} N m up to a 50 m reflector size, which can be easily supplied by a small DC motor. For the range of reflector size considered here, the total mass is below 100 kg, below the maximum 120 kg mass allowed for a BEXUS experiment [14].

It seems that a 20 m reflector is a reasonable choice for this demonstration (deployement of a sail with similar size was also proposed in Ref. [15]), providing a peak power density of approximately 14 W m^{-2} and requiring approximately 1×10^{-4} N m of control torque, for a total reflector mass of approximately 15 kg. Assuming a total solar panel area on the ground of 10 m^2 and a 20% energy conversion efficiency the total power on the ground is approximately 28 W, enough to power a small light bulb. Using the equations provided in Ref. [6] it can be shown that the light ellipse on the ground has semimajor and semiminor axes of approximately 50 m and 40 m, respectively and therefore a 10 m^2 square target is fully contained within the light ellipse assuming correct target pointing. In principle, if the entire ellipse area is covered by solar panels (e.g., the reflector is illuminating an existing solar power farm), the maximum power that can be generated is up to three orders of magnitude larger, approximately 46 kW.

One possible issue related to this demonstration is

due to the oscillations of the gondola caused by unexpected wind gusts. In the next section an estimate of such oscillations is made, assuming a change in the wind speed, taking key strctural reference parameters from Ref. [14].

2.3 Gondola oscillations caused by wind gusts

In this section, a simple model is developed to analyse the effect of wind gust on the balloon and gondola structure.

The balloon and gondola are modelled as two point masses connected by a massless cable with length L. It is assumed for simplicity that the balloon vertical velocity is constant. Consider an inertial reference frame which is initially centred at the balloon centre-of-mass and moving vertically towards the positive y-axis with constant velocity (equal to the ascent velocity). Let $\mathbf{r}_r = (x_r, y_r)$ and $\mathbf{r}_b = (x_b, y_b)$ be the position vector of the reflector and the balloon with respect to the inertial reference frame, respectively. The coordinates of the reflector can therefore be expressed as:

$$x_r = x_b + L\sin\theta \tag{7}$$

$$y_r = -L\cos\theta \tag{8}$$

Given that the reflector is ascending with constant velocity it follows that:

$$y_b = 0 \tag{9}$$

$$\dot{y}_b = 0 \tag{10}$$

Therefore, the system can be characterized by only two degrees of freedom, in this case the horizontal balloon displacement x_b and the gondola rotation angle θ. The total kinetic energy T is the sum of the balloon and gondola kinetic energies, i.e., :

$$\begin{aligned} T &= \frac{1}{2}m_b\dot{x}_b^2 + \frac{1}{2}m_g(\dot{x}_r^2 + \dot{y}_r^2) \\ &= \frac{1}{2}m_b\dot{x}_b^2 + \frac{1}{2}m_g(\dot{x}_b^2 + L^2\dot{\theta}^2 + 2L\dot{x}_b\dot{\theta}\cos\theta) \end{aligned} \tag{11}$$

By neglecting the change of the gravitational constant due to altitude (this is a reasonable assumption given the low altitudes reached by the balloon), the total potential energy can be written as:

$$U = m_g g L(1-\cos\theta) \tag{12}$$

The Lagrangian of the system can therefore be written as:

$$\begin{aligned} L &= T - U \\ &= \frac{1}{2}m_b\dot{x}_b^2 + \frac{1}{2}m_g(\dot{x}_b^2 + L^2\dot{\theta}^2 + 2L\dot{x}_b\dot{\theta}\cos\theta) \\ &\quad + m_g g L\cos\theta \end{aligned} \tag{13}$$

The external forces acting on the system are the drag force on the balloon and the the reflector. For simplicity, the torque due to the motor steering the reflector is neglected. Assuming small oscillation of the gondola, these can be modelled as:

$$F_b = k_b(\dot{x}_b - v_w)^2 \tag{14}$$

$$F_r = k_r(\dot{x}_r - v_w)^2 \tag{15}$$

where v_w is the wind velocity and the the coefficients k_b and k_r are

$$k_b = \frac{1}{2}C_{d,b}A_b\rho_{\text{atm}} \tag{16}$$

$$k_r = \frac{1}{2}C_{d,r}A_r\rho_{\text{atm}} \tag{17}$$

The terms $C_{d,b}$ and $C_{d,r}$ are the drag coefficients of the balloon and reflectors respectively, A_b and A_r are their cross section areas and ρ_{atm} is the atmospheric density. In this and following sections, the atmospheric density is calculated using the NRLMSISE-00 model [16], assuming low solar activity. The generalised forces can therefore be written as:

$$Q_x = F_b\hat{\mathbf{i}}\cdot\frac{\partial\mathbf{r}_b}{\partial x_b} + F_r\hat{\mathbf{i}}\cdot\frac{\partial\mathbf{r}_g}{\partial x_b} \tag{18}$$

$$Q_y = F_r\hat{\mathbf{i}}\cdot\frac{\partial\mathbf{r}_g}{\partial\theta} + F_r\hat{\mathbf{i}}\cdot\frac{\partial\mathbf{r}_g}{\partial\theta} \tag{19}$$

The equations of motion can therefore be written in Lagrangian form as

$$\begin{cases} \dfrac{d}{dt}\left(\dfrac{\partial L}{\partial\dot{x}_b}\right) - \dfrac{\partial L}{\partial x_b} & = Q_x \\ \dfrac{d}{dt}\left(\dfrac{\partial L}{\partial\dot{\theta}}\right) - \dfrac{\partial L}{\partial\theta} & = Q_\theta \end{cases} \tag{20}$$

Substituting Eqs. (18) into Eqs. (20) and simplifying, the equations of motion can finally be written as:

$$\begin{Bmatrix} (m_r+m_g) & \cos\theta \\ \cos\theta & L \end{Bmatrix}\begin{Bmatrix} \ddot{x}_b \\ \ddot{\theta} \end{Bmatrix} = \mathbf{b} \tag{21}$$

where

$$\mathbf{b} = \begin{Bmatrix} F_b + F_r + \dot{\theta}^2\sin\theta \\ \dfrac{F_r}{m_g}\cos\theta + \dot{x}_b\dot{\theta}\sin\theta - (g+\dot{x}_b\dot{\theta})\sin\theta \end{Bmatrix} \tag{22}$$

Solutions to Eq. (21) are now presented by fixing the following parameters: $A_b = 2.94\times10^3\,\text{m}^3$, $L = 50\,\text{m}$, $C_{d,b} = 0.5$, $C_{d,r} = 2.2$, $m_b = 110\,\text{kg}$. The area of the balloon is chosen assuming a spherical balloon with total volume as indicated in the BEXUS handbook. Similarly, the cable length and balloon mass

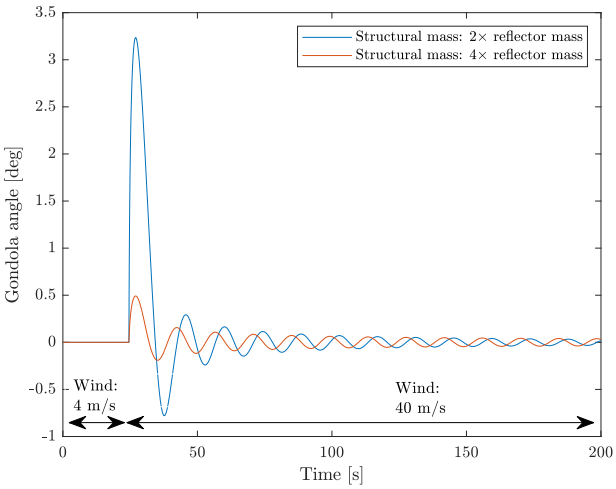

Fig. 9: Effect of wind gusts on the gondola angle. The initial wind speed is $4\,\mathrm{m\,s^{-1}}$. At $t = 40\,\mathrm{s}$ a wind gust is simulated setting $v_w = 40\,\mathrm{m\,s^{-1}}$.

are taken from the BEXUS handbook. For simplicity, it is assumed that the the drag coefficient of the reflector is constant and equal to that of a plate moving parallel to air flow direction. Figure 9 shows the gondola angle as a function of time, assuming a step change of the horizontal wind speed from $4\,\mathrm{m\,s^{-1}}$ to $40\,\mathrm{m\,s^{-1}}$. Responses for different structural masses are shown. The structural mass is the sum of all the components excluding the reflective membrane and inner frame (e.g., reaction wheel, external frame, sensors, motors). As expected the oscillation are larger with a smaller structural mass, with peak oscillation amplitudes of approximately 3°. The period is approximately equal to the period of the simple pendulum $2\pi\sqrt{L/g}$, in this case approximately 15 s. It is therefore expected that for wind speed changes up to $40\,\mathrm{m\,s^{-1}}$ the system does not exhibit unstable behaviour, although additional issues related to the reflective membrane wrinkling or damaging may emerge.

2.4 Sounding rocket demonstration

The primary objectives of the sounding rocket demonstration are:

- Perform a reorientation manoevure in microgravity conditions and redirect sunlight towards a light sensor on the ground.
- Study the effects of membrane deformation due to the control manoeuvre.
- Study the membrane deployment.

Table 2: Main specifications of some sounding rockets. Rexus and S-310 were used to launch experiments involving membrane deployment.

	Apogee	Diameter	Payload mass
Rexus	80 km	0.35 m	95 kg
S-310	150 km	0.31 m	50 kg
Texus	260 km	0.57 m	260 kg
Maxus	705 km	0.64 m	480 kg

- Validation of the models for atmospheric losses, with light reflection through the entire atmosphere.

The proposed mission concept is shown in Fig. 10. After burnout the payload is released from the nose cone and the reflective membrane is immediately deployed, such that the reflector normal is perpendicular to its velocity, to minimize the effect of the air drag. Then the payload attitude is stabilized after the deployment and the reflector is gradually slewed in order to reflect sunlight to a ground target when close to the apogee. In order to simplify the calculations and easily estimate the required manoeuvre torques, a bang-bang manoevure is assumed. Eventually, the contact is maintained as the reflector descends through the upper stages of the atmosphere and the payload is then safely recovered with a controlled re-entry via parachute. The optimal sounding rocket apogee altitude will ultimately depend on the desired level of stresses of the membrane upon deployment, due to the atmospheric drag. Clearly, at higher altitudes the atmospheric density is lower thus decreasing the drag forces on the deployed membrane, however, the illumination on the ground will be reduced as dictated by the power law (6). Past experiments involving membrane deployment include a $2\,\mathrm{m}^2$ drag sail demonstrator launched on a Rexus rocket [17]. The sail successfully deployed however it quickly collapsed upon beginning of the descent due to the aerodynamic drag. Another experiment involved the deployment of a 10 m diameter sail from a S-310 rocket, with a higher apogee altitude of 150 km [15]. The sail deployed as expected, although there was no attempt to perform an attitude control manoeuvre on the sail.

The effects of the atmospheric pressure acting on the membrane can be investigated using free molecular flow theory [18]. In particular, assuming a flat plate in a free molecular flow, the resulting force depends on the angle of attack in the form:

$$F_D = \frac{1}{2}\rho v^2 A C_D \tag{23}$$

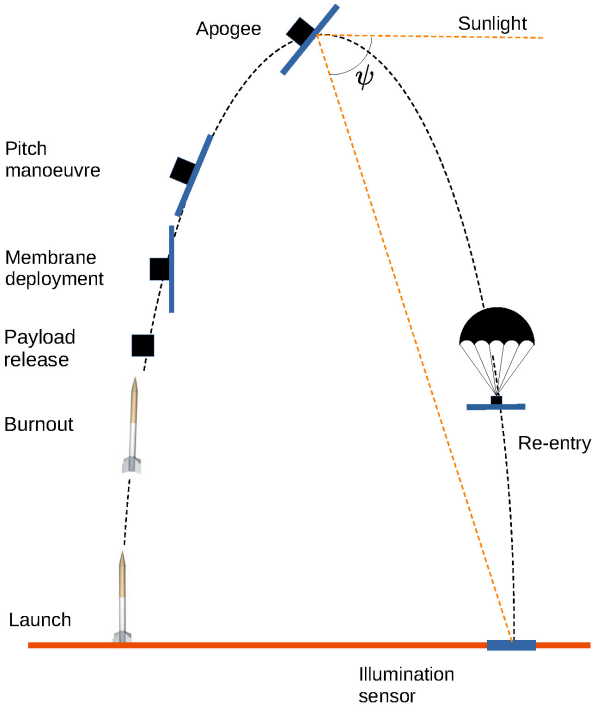

Fig. 10: Sounding rocket demonstration concept.

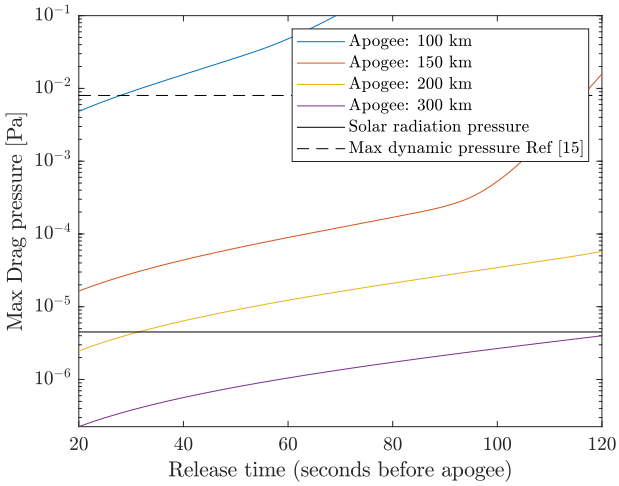

Fig. 11: Maximum dynamic pressure on a flat plate as a function of its side and the release time (taken as Δt with respect to the apogee).

where the drag coefficient C_D can be expressed as [18]:

$$C_D = 2\left[\sigma_t + \sigma_n \frac{w}{v}\sin\beta + (2-\sigma_n-\sigma_t)\sin^2\beta\right]\sin\beta \tag{24}$$

where σ_n, σ_t are coefficients taking into account the momentum exchange of the incoming particles in the normal and tangential direction (*momentum accommodation coefficients*) and w is the average normal velocity of the particles impinging on the surface [18]. The lift coefficient is usually much smaller than the drag coefficient and the effect of the lift can therefore be neglected [18]. Furthermore, contrary to a flat plate in a high-density continuum flow, the centre of pressure coincides with the centre-of-mass, hence the net torque due to aerodynamic forces with respect to the centre-of-mass is zero. Clearly, in this case the reflector will not be perfectly flat due to possible membrane wrinkling, boom deformation upon deployment and due to the presence of the central payload bus, which will change the geometry of the experiment. However, it is reasonable to assume that the reflective membrane will be much larger than the payload bus.

Figure 11 shows the maximum drag pressure acting on the reflector (modelled as a flat plate for simplicity), as a function of the release time (taken as the time difference from apogee) and of the apogee altitude. As discussed, it is assumed that the reflector is deployed with zero angle of attack and then it is pitched until reaching the desired angle of attack which guarantees reflection of sunlight to the ground target. For apogee altitudes below 200 km the maximum drag pressure is always larger than the solar radiation pressure, assuming release times between 20 and 120 seconds before apogee. The analysis in Ref. [15] considered a maximum dynamic pressure of 8×10^{-3} Pa. Results in Fig. 11 suggest that apogee altitudes should be higher than 100 km to guarantee peak pressures lower than this value.

While higher altitudes ensure lower dynamic pressure, the illumination level will be lower for sunlight reflection from the upper atmosphere. The illumination level on the ground in lux can be expressed as [8]:

$$P_{lux} = I_{lux}\frac{A_r}{A_{im}}\cos\frac{\psi}{2} \tag{25}$$

where I_{lux} is the solar power density in lux which can be approximated to $I_{lux} \approx 100\,000$ lx taking into account atmospheric losses [8]. Assuming vertical ascent of the rocket, the angle ψ between the incoming and reflected sunlight is:

$$\psi = \frac{\pi}{2} - \arccos\frac{h}{\sqrt{h^2+d^2}} \tag{26}$$

where h is the rocket altitude and d is the distance between the launch site and the target. Figure 12 shows the illumination level on ground as a function

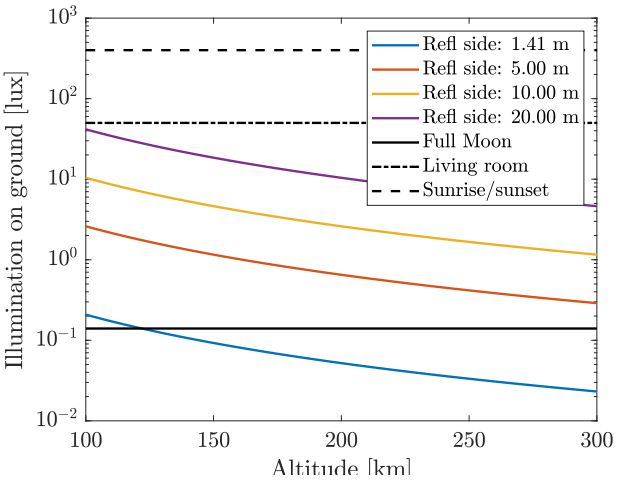

Fig. 12: Illumination of ground (in lux) as a function of the altitude, for different reflector sizes.

of the sounding rocket apogee altitude (the illumination is measured at the apogee) and the reflector side. Here, it is assumed that $d = 0$, such that the pitch angle is constant and equal to 45 deg (this assumption clearly does not take into account the horizontal displacement of the rocket however it is expected that the vertical range is much larger than the horizontal range [19]). It is apparent that using a $2\,\mathrm{m}^2$ sail as in Ref. [17] would produce illumination levels lower than the full Moon level (0.14 lx) for virtually any apogee altitude above 100 km. On the contrary, illumination levels larger than living room levels (50 lux) can only be reached with reflectors larger than 20 m. Note that by increasing the horizontal distance between the target and the reflector at the apogee, the angle ψ, decreases hence, from Eq. (25) the illumination increases. However, at the same time, the area of the image of the ground also increases, which reduces the illumination. It can be shown that for an apogee altitude of 260 km the optimal distance to maximize the illumination on the ground is approximately 40 km. However, note that the illumination only increases from 1.54 lx to 1.6 lx, hence the change is not significant.

At higher altitudes, e.g., Maxus apogee altitude, the illumination level is extremely low. A 10 meter reflector would barely reach a full moon illumination level making the detection more challenging. Furthermore, higher pointing precision would be required.

In the following, it is assumed that a Texus sounding rocket is used to deploy a 10 m side square reflector from a CubeSat, with estimated apogee at an altitude of 260 km. From Fig. 12, the expected illumination level at at the apogee will be one order of magnitude larger than the full moon illumination level, approximately at 1.5 lx, enough to be detected by high sensitivity light sensors* To estimate the membrane mass, values from Ref. [17] are used. In particular, the combined membrane mass and boom mass was 450 g for a $2\,\mathrm{m}^2$ drag sail, i.e., corresponding to an areal density of $125\,\mathrm{g\,m^{-2}}$. In the following analysis an areal density of $200\,\mathrm{g\,m^{-2}}$ will be used for a baseline 10 m square reflector.

2.4.1 Preliminary actuator sizing

Assume that a set of three reaction wheels is used for three-axis control of the payload upon membrane deployment. To estimate the required wheel size, it is assumed that all three wheels are sized based on the pitching reorientation manoeuvre. First, assuming a bang-bang reorientation manoeuvre, the required control acceleration for the pitching manoeuvre can be estimated from

$$\ddot{\theta} = \frac{2\pi}{(\Delta t/2)^2} \tag{27}$$

and, therefore a total torque

$$T = \ddot{\theta} J \tag{28}$$

where Δt is the total manoeuvre time (i.e., from membrane deployment to the apogee) and J is the in-plane reflector inertia. For a 10 m reflector, the required torque is approximately $36 \times 10^{-3}\,\mathrm{N\,m}$. Note that this is 6 orders of magnitude less then the torque required for the full scale structure.

Assuming that the actuator mass is calculated from Requirement RC3, i.e., being 60% of the membrane mass. Then, modelling the reaction wheel as a disk with radius r_w and tickness t_w and density ρ_w, the required radius is

$$r_w = \sqrt{\frac{m_w}{\rho_w \pi t_w}} \tag{29}$$

Then taking a wheel thickness of 1 cm yields yields a wheel radius of $r_w = 13\,\mathrm{cm}$. The required wheel angular momentum can then be estimated:

$$H_w = T\frac{\Delta t}{2} = 2.18\,\mathrm{N\,m\,s} \tag{30}$$

and therefore, the maximum wheel angular velocity:

$$\omega_w = \frac{T}{I_w}\frac{\Delta t}{2} = 655\ \mathrm{RPM} \tag{31}$$

*See, e.g., https://dcfa.exa.unicen.edu.ar/wp-content/uploads/sites/18/2019/02/Spectrophotometer_b.pdf, accessed on 18 August 2022.

The wheels can be placed inside the CubeSat structure and can be powered by DC motors.

2.5 In-orbit demonstration

This phase of technology demonstration aims to validate the concept as a full-functional spacecraft in orbit, unlike the specific issues that are aimed to be validated in high-altitude balloons or sounding rockets. The objectives of in-orbit demonstration phase can be summarised as follows:

- Performing a full system level space operation in orbit for a reflector spacecraft.
- Pointing to and tracking a solar power farm throughout an orbital pass over a solar power farm.
- Illuminating a solar power farm or farms for electricity generation.
- Measuring the intensity of solar power on the ground.
- Validating the analytical models related to the power received on the ground.
- Understanding the efficiency of light reflection at lower elevations.

The reflector spacecraft in orbit, regardless of its size, will include a full spacecraft bus and the reflector as its payload. The in-orbit demonstration phase will allow for validating the full system-level performance. A particularly important aspect of the in-orbit demonstration is to perform attitude control manoeuvres to point and track solar power farms. Attitude control is demonstrated to be a particularly demanding part of operating the reflectors [6, 8]. Attitude control errors may result in inaccuracies in the direction reflected light, which would affect both the energy generated and stray light considerations. Therefore, the validation of in-orbit attitude control is essential. Attitude control in this phase is directly related to the light that is reflected. It is envisaged that electricity generation will be attempted from a solar power farm. Albeit potentially in small quantities, electricity generation via light reflected from space will be a proof of the concept. Further intensity measurements will be made through light sensors on the ground, and more qualitative observations will be made via the camera images taken of the solar image on cloud tops. The former will allow for validating the analytical models of solar energy delivery from space [6], particularly in terms of atmospheric losses and cloudiness, which is not well quantified thus far. The latter will validate the expected shape of the reflected solar image and the impact of non-idealities, e.g. reflector wrinkling, on this shape.

Table 3: Orbital element of the ISS On July 29, 2022.

Element	Value
Semi-major axis	6793.76 km
Eccentricity	0.0005
Inclination	51.64 deg
Right Ascension of the ascending node	128.56 deg
Argument of perigee	15.50 deg

The first step considered is a CubeSat-type reflector spacecraft, deployed from the KIBO module of ISS. This is motivated by the fact that no dedicated or piggy-back launches are necessary. A CubeSat can be built relatively quckly and at an altitude of approximately 400 km, it would allow for relatively rapid deorbiting for debris mitigation. Technology now allows for solar sails to be stowed and deployed from CubeSats, as evidenced by the Planetary Society's successful operation of the LightSail CubeSat [20]. Orbiting solar reflectors are essentially the same technology, therefore the LightSail's 31.36 m^2 sail [20] will be considered to be the smallest reflector size to be tested in space. During operations, some of the largest solar power farms could be illuminated, listed in Ref. [8]. The orbit of the reflector spacecraft is assumed similar to the orbit of the ISS, hence the five constant orbital elements of the ISS are used for propagation as provided in Table 3[†]: The orbit is propagated numerically for 7 days by also including the Earth's oblateness up to the second degree, i.e., J_2 [21]. Deorbiting due to air drag is ignored at this stage for simplicity. The ground track of the propagated orbit is presented in Fig. 13. The initial position of Greenwich meridian is arbitrarily selected for the generation of the ground track. Figure 13 also depicts the locations of the solar power farms considered. Qualitatively, it can be seen that the orbit passes over all the solar power farms. It is discussed previously that the maximum elevation achieved should be at least 60 deg for a reasonable quantity of energy to be delivered [8]. Another consideration is whether the orbital passes shown in Fig. 13 are when the reflector is in the Earth's shadow. This is analysed by investigating the spacecraft contacts by including the Earth's shadow cone and constraining the contact locations

[†]Available here `https://www.heavens-above.com/orbit.aspx?satid=25544`, accessed July 29, 2022.

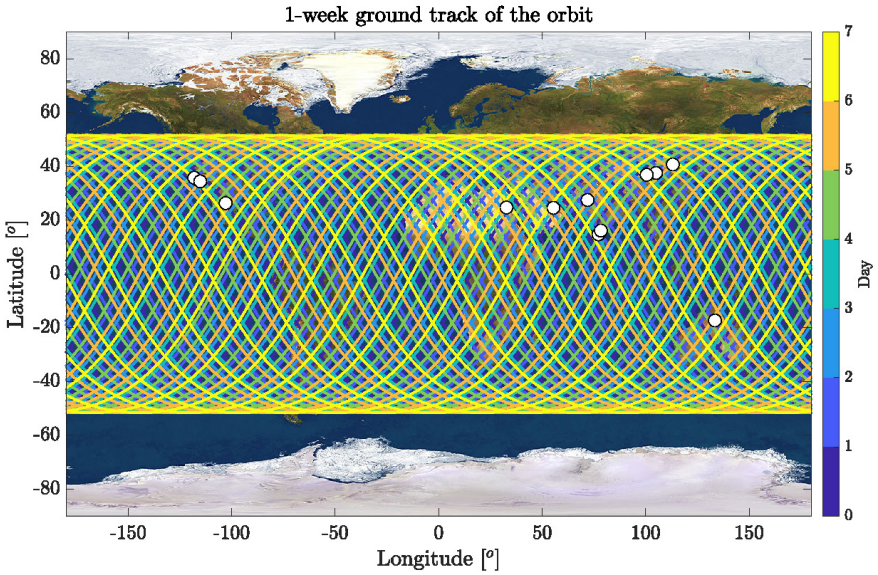

Fig. 13: 1-week ground track of a reflector in an ISS-like orbit.

near dawn/dusk hours, as shown in Fig. 14. An angle β can be defined to find longitude after which the reflector will be in the Earth's shadow as

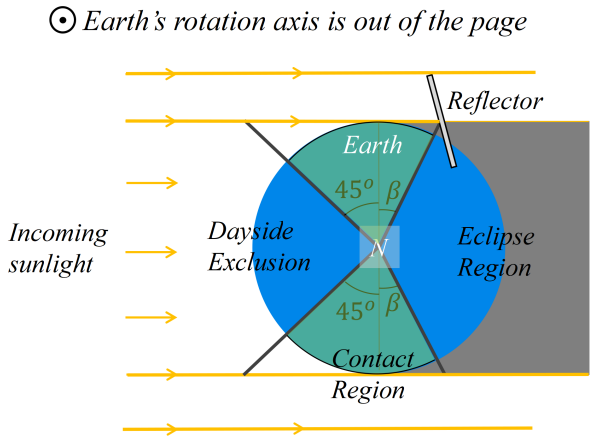

Fig. 14: The dawn/dusk regions of contact sought between the reflector spacecraft and solar power farms.

$$\beta = \arccos\left(\frac{R_E}{R_E + h}\right) \tag{32}$$

where $R_E = 6378.2\,\text{km}$ is the Earth equatorial radius and h is the orbit altitude. β is approximately 20 deg for the altitude of 416.35 km considered here. An additional 45 deg is assumed to exclude a part of the dayside of the Earth, as well, to achieve dawn/dusk solar energy delivery and improve the measurability of the delivered sunlight. The 60 deg criterion is achieved for all solar power plants for 1 week of operation within this contact region.

In order to investigate the visibility of the solar power farms and the energy delivery properties in a more quantitative manner, the numerical propagator is expanded to include the energy delivery as the 7th parameter to the equations of motion. At each step of the numerical integration, the position of the reflector is projected onto a topocentric frame defined on the selected solar power farm. If the elevation angle is greater than 0 deg (i.e., the reflector spacecraft is in view), Eq. (6) is used to calculate the power delivered. The image area A_{im} and the angle ψ are calculated at each integration step. Ultimately, the energy delivered is calculated as:

$$E = \int_0^{T_{\text{pass}}} P(t)\text{d}t \tag{33}$$

during the numerical propagation, where E is the energy delivered and T_{pass} is the duration of the pass. The details of the calculation process are provided in Ref. [6]. If the elevation angle is smaller than 0 deg, then $P = 0$. This procedure considers the desired contact region discussed earlier, but it does not include the maximum elevation criterion of 60 deg, hence the output provides an upper limit to the energy delivered to a selected solar power farm. The results are shown in Fig. 15. The reflector area is

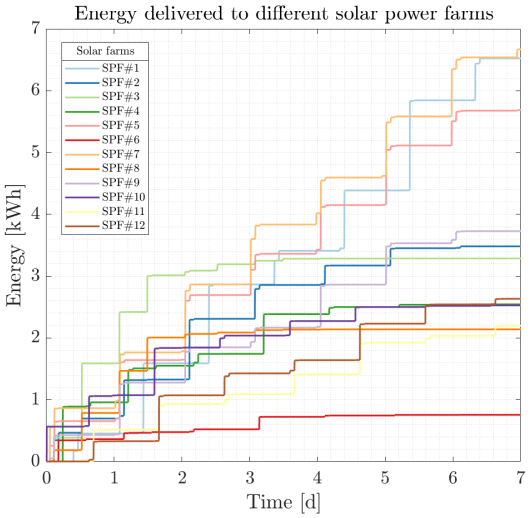

Fig. 15: Total energy delivered to each solar power farm by a 31.36 m^2 solar reflector (equivalent to that of the LightSail CubeSat) to each visible solar power farm (no minimum elevation criterion)

equal to 31.36 m^2, as noted before. The currently existing area values for the solar power farms are used, but they are considered circular, as per the calculation procedure [6]. Figure 15 depicts a stairs-type plot with instantaneous jumps in the quantity of energy delivered. The jumps are in fact not instantaneous, but the pass duration (approximately 10.4 min) for the selected orbit altitude is much shorter than the simulation duration. Small increases in the quantity of energy delivered are due to low elevation passes, which are not discarded in the current paper, as noted earlier. It must be noted that, contrary to the analysis in Ref. [8] for the full-scale case, constraints on the reorientation time are not considered here but will need to be addressed in a future analysis. According to Fig. 15, there appear to be daily visits to almost all targets, although there are fewer opportunities for some of the other farms after the 4th day of operations. The maximum energy delivery is approximately 6.7 kWh to both Datong and Sun Cable solar power farms, and the minimum is approximately equal to 1 kWh (note that these values are not a result of an optimisation selection of the ground track and could change by selecting a different position of the Greenwich meridian at $t = 0$). Note that this is the total energy delivered to the target before the conversion losses. If it is assumed that the efficiency of solar cells is 20% and the ground coverage ratio is 50% then the converted energy into electricity is equal to approximately 10% of the values presented in Fig. 15. This is clearly not high, but it can demonstrate that the concept of orbiting solar reflectors is feasible to be utilised.

Indeed the results presented in Fig. 15 are scalable to larger reflectors. From Eq. 6, for a given orbit, atmospheric losses and the area of the solar image is the same for all reflectors with the point-mass reflector assumption, which is valid for small reflectors [6]. If the reflectivity of the reflectors is the same, the only property that changes the power delivered is the area of the reflector. Then, a linear scaling coefficient can be defined to calculate the energy delivered by larger reflectors as

$$\kappa = \frac{A_r}{A_*} \tag{34}$$

where κ is the scaling coefficient, A_* is the energy delivered by the reference reflector area, in this case, the LightSail CubeSat's 31.36 m^2. At this point, several different reflector areas will be considered. As another example of a solar sail experiment, the IKAROS spacecraft is considered, which has a sail area of 196 m^2 (14 m × 14 m). From the scaling relationships in Eq. 2.5, $\kappa = 6.25$, hence the delivered energy would be 6.25 times increased.

The other examples will also be taken from technology demonstration attempts. The Znamya-2 experiment is the closest example to the concept discussed here. The 20-m diameter reflector was deployed in 1993 from the Mir space station during the Russian "New Light" experiment with an aim to demonstrate the technologies of solar sailing and orbiting solar reflectors [22]. The subsequent Znamya-2.5 experiment with a diameter of 25-meter failed during deployment [23]. The Znamya-3 experiment, which was planned to deploy a 70-meter diameter reflector, was cancelled subsequently. The Znamya and SolarKraft projects by the Russian Space Regetta Consortium aimed at progressively increasing the sizes of reflectors up to 200 m in diameter[‡], as similarly considered here. These reflector sizes are assumed and the quantities of energy delivered for each are presented in Table 4. The linear scaling in Table 4 shows that considerable quantities of energy can be delivered even with an IKAROS-type reflector. For the largest size of reflectors, nearly a MWh-level of energy can be delivered. Once again note that this is the quantity of solar energy before the conversion losses during electricity generation, which is assumed

[‡]See `https://web.archive.org/web/20060808175720/http://www.space-frontier.org/Events/Znamya/`, accessed on July 29, 2022

Table 4: Scaled quantity of energy delivered and required control effort (angular momentum and torque) for different reflector sizes

Example	Dimensions	κ	$E_{\max}$ [kWh]	Ang. momentum	Torque
LightSail	$5.6\,\mathrm{m} \times 5.6\,\mathrm{m}$	1	6.67	$9.2 \times 10^{-2}\,\mathrm{N\,m\,s}$	$1.1 \times 10^{-3}\,\mathrm{N\,m}$
IKAROS	$14\,\mathrm{m} \times 14\,\mathrm{m}$	6.25	41.69	$3.6\,\mathrm{N\,m\,s}$	$4.3 \times 10^{-2}\,\mathrm{N\,m}$
Znamya-2	$\varnothing 20\,\mathrm{m}$	10.02	66.83	$2.8\,\mathrm{N\,m\,s}$	$3.4 \times 10^{-2}\,\mathrm{N\,m}$
Znamya-2.5	$\varnothing 25\,\mathrm{m}$	15.65	1404.39	$6.8\,\mathrm{N\,m\,s}$	$8.1 \times 10^{-2}\,\mathrm{N\,m}$
Znamya-3	$\varnothing 70\,\mathrm{m}$	122.72	818.54	$4.2 \times 10^{2}\,\mathrm{N\,m\,s}$	$5\,\mathrm{N\,m}$

to be approximately 10% in total. Table 4 also shows the required control effort for each reflector size. The required angular momentum and torque are calculated assuming an ideal overhead pass at the designated ISS orbit altitude, using the method described in Ref. [9]. Additional details about the reflector attitude during the targeting manoeuvre can be found in Ref. [9]. Since the inertia of the reflector scales with the fourth power of its size [9, 8], the required angular momentum and torque are several orders of magnitude smaller than the nominal values for the full-scale 250 m strucutre. A reduced-scale version of the CMG cluster discussed in Ref. [8] can be used for attitude control in this case. For dimensions up to 25-meter diameter, standard off-the-shelf CMGs for CubeSats can be used to generate the required angular momentum and torque [24].

As for solar power density on the ground, previous work discussed that the maximum solar power density at 400 km would be approximately 2 lux for a 20-meter diameter reflector [5], which is measurable by light sensors, as noted earlier in this paper. The κ-scaling would also work in this case and it can be found that the same light sensors could also measure the power density from the IKAROS-type reflector case, where $\kappa \approx 0.62$ with respect to the 20-m diameter case. The smallest reflector would deliver the maximum solar power density of 0.199 lux ($\kappa \approx 0.099$), which is higher than the full moon intensity (0.143 lux [3]). It would be harder to detect this level of intensity, but such sensitive light sensors exist as noted earlier. It is known that some electricity can still be generated from solar power farms under full-moon conditions The measured quantities can then be compared against theoretical models to better understand the atmospheric transmission of solar energy.

It can be argued that large reflectors such as 20-m diameter cannot be packed into a CubeSat. One possible alternative is to use multiple CubeSats to allow deployment opportunities from the ISS. This is also proposed for larger reflector spacecraft to maximise the quantity of energy delivered while easing the attitude control requirements [8]. Another alternative could be to deploy the reflectors from departing ISS servicing spacecraft, such as SpaceX's Dragon capsule. This would be a scenario similar to the Znamya-type experiments, which were deployed from the Mir space station by a motor attached to the Progress supply spacecraft [22]. The advantage with such a scenario is that large attitude control torques for orientation can be counteracted by the thruster-based attitude control systems available in such servicing spacecraft, which may not be feasible for smaller spacecraft. They can also be deployed from similar altitudes as the ISS or lower, to maximise the measurability of the quantity of solar energy delivered.

Finally, for all the concepts presented, once the mission is completed it will be de-orbited to burn up in the atmosphere. This can be achieved by using the reflector as a drag sail. Even without a drag sail, the lifetime of an uncontrolled spacecraft is on the order of months at the envisaged altitude of approximately 400 km. Using a drag sail will only make the lifetime shorter. Indeed, Surrey Space Center's InflateSail deorbited from an initial perigee altitude of 550 km altitude to below 250 km by deorbiting in 72 days by using a $10\,\mathrm{m}^2$ square drag sail [25]. The CubeSat-type reflector spacecraft envisaged in this paper will not actively face the ram direction to deorbit while in operation, but it will have a larger reflector and lower altitude. As the reflector spacecraft is performing its operations, the quantity of energy delivered will increase with decreasing altitude, but a dedicated analysis of the deorbiting process is left for future studies.

3. Timescale and investment profile

Space technological innovations are categorised using a Technology Readiness Level (TRL) scale with

Table 5: The Technology Readiness Level (TRL) scale used to judge new space technologies.

TRL Level	Expectation
9	Actual system proven in operational environment
8	System complete and qualified
7	System prototype demonstration in operational environment
6	Technology demonstrated in relevant environment
5	Technology validated in relevant environment
4	Technology validated in laboratory environment
3	Experimental proof of concept
2	Technology concept formulated
1	Basic principles observed and reported

nine distinct levels. For a technology to be considered fully matured and ready for commercialisation, such technology must have successfully passed through all levels on the TRL scale. The TRL is summarized in Table 5. The TRL 1 and 2 have been achieved through the numerous publications that have proven the concept of orbiting solar reflectors. Some key publications are discussed in Section 1

In this study, four technology demonstration phases for the commercial development of orbiting solar reflectors are discussed. The timelines within each phase and the potential cost of each phase are further discussed.

1. Laboratory demonstration

   The first phase in the technology demonstration for commercial deployment of orbiting solar reflectors is the laboratory scale testing and demonstration phase. In the laboratory, various sets of tests will be carried out on different sub systems of the reflector. Tests on different suitable materials for the reflector surface, tube strength and interconnection for the reflector structure and reflector control mechanism. As highlighted in Table 1, these tests are essential to ensure that the reflector will satisfy the control, structural and manufacturing requirements.

   The laboratory demonstration phase will be carried out within an estimated period of 48 months and at an estimated cost of £15 million. The larger percentage of costs incurred in this phase is related to the construction and testing of the subsystems of the reflector and the entire reflector architecture.

   This phase will culminate in the production of complete scaled reflector prototypes of different sizes. TRL 3 and 4 is achieved with the laboratory demonstration.

2. Stratospheric (High Altitude) balloon demonstration

   For this phase, a small sized reflector (such as a 5-metre reflector) will be attached to the gondola of a helium filled balloon which is then launched to high altitudes. This phase aims to demonstrate the reflector operations at altitudes just below the space boundary. During the flight, the ability of the reflector's control mechanism to maintain focus to a location on Earth and its energy transfer efficiency will be analysed.

   It is estimated that this phase will be carried out over a period of 30 to 36 months. This will involve two demonstration flights and other activities such as detailed analysis to determine a suitable target location based on the balloon launch site; production of a 20-metre sized reflector to be used for the flight; the installation of illumination measuring devices at the target location.

   The first flight will be between month 9 and month 12. Preparation for the first flight is expected to take between six to eight months. The time and day of the balloon flight can only be decided in consultation with the balloon flight launch company.

   Following the flight, analysis of illumination measurements and the impact of different factors such as flight path and wind direction will be carried out. The analysis is estimated to take approximately six months, the results of this analysis will influence the necessary adjustments and improvements to the reflector configuration and the entire process for the second balloon demonstration flight which is estimated to take place by month 28. The successful completion of this phase achieves TRL 5 and contributes towards achieving TRL 6.

3. Sounding Rocket Flight

   Since the balloon demonstration flight does not ascend into the space environment, the sounding rocket flight is the first opportunity to test the full functionality of the reflector. In this

phase, the following aspects will be tested: deployment mechanism for the reflector; reflector surface wrinkling in space; energy transfer capacity of the reflector from space. In Table 2, four sounding rocket programs were highlighted. Three of these four programs are carried out by the European Space Agency (ESA). After ESA approves an experiment for a sounding rocket flight, a period of 2 to 3 years is typically required to prepare for the flight [26].

After the successful balloon demonstration flight, it is estimated that experiment will receive approval for a sounding rocket flight within six months, preparation for the flight is estimated to take two and a half years (thirty months), eighteen months to fully analyse the results obtained during the flight demonstration and for further development of the reflector. A second flight is estimated to take place three years after the first flight. Analysis of results would take the last one year.

On successful completion of the result analysis, the system will be complete and qualified for demonstration in an operational environment. The sounding rocket flight demonstration phase is estimated to cover a period of 4 years and will achieve the technology readiness levels 6, 7 and 8.

4. In Orbit demonstration

This phase involves the deployment of reflector for operations to illuminate the target locations on the Earth. The effectiveness of the reflector control mechanism; the impacts of cloud cover on the reflector energy transfer efficiency; the periodicity of the time of reflector illumination across multiple days will be analysed.

The in-orbit demonstration phase can be designed to have two stages. The first stage can involve the use of a CubeSat to deploy a small sized reflector in space. This is advantageous as it allows testing of the reflector technology at a lower cost. The CubeSat in-orbit demonstration can take place just after the sounding rocket flight is concluded. The analysis of the result obtained from CubeSat in-orbit demonstration will be useful to understand the needed improvements in designing the larger sized reflector to use in the next stage of the in-orbit demonstration.

The next stage of the in-orbit demonstration is envisaged to involve two flights and will be carried out over a period of 6 to 7 years. The solar power satellite concept, which is a significantly heavier and more complicated space system [5], is estimated to require eight years for small scale and full-scale in orbit demonstration of the technology [27]. Owing to this, we have estimated that the medium sized reflector of 100m length will be demonstrated in year 2 and a full-scale demonstration of a constellation involving three 250 metre sized reflector in year 5. The analysis of all results obtained from the flight will take an estimated period of eighteen months.

The successful in-orbit demonstration will confirm the full maturity of the technology for commercialisation.

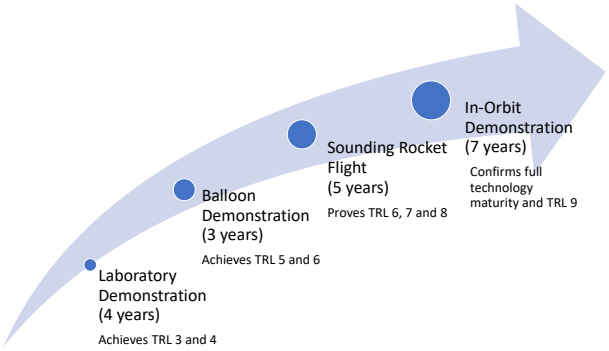

Fig. 16: Estimated timeline for the different demonstration stages

4. Conclusions

In this paper a technology demonstration roadmap for orbiting solar reflectors has been presented. Based on specific requirements for a full-scale mission, key laboratory tests have discussed which will validate key technology aspects.

First, laboratory-scale demonstration tests are considered to validate structural models for loads, study membrane flatness and tensioning, determine the effects of thermal expansion, perform microgravity tests for in-space additive manufacturing and test the actuator.

Then, high-altitude balloon tests have been discussed. A 20 m reflector attached to the gondola of a high-altitude balloon will directly illuminate a solar power target on the ground, thus validating analytical models related to the power density and solar image on ground, understand the efficiency of light reflection at lower elevations and validate the models for atmospheric losses. It was shown that a 20 meter

reflector attached on a gondola can deliver sufficient power to light up a small light bulb using a $10\,m^2$ solar panel target.

Deployment of a small-scale reflector from a sounding rocket is then discussed. A 10 m square reflector launched from a sounding rocket with apogee at 260 km is proposed. The reflector dimension and rocket apogee were selected based on a trade-off between drag pressure and illumination on the ground. It is shown that the illumination level on the ground at the apogee is on the order of 1 lx, very small but enough to be detected by a light sensor array.

An in-orbit demonstration was then discussed, aiming at tracking a solar power farm throughout an orbital passage over a solar power farm and performing a full system level space operation in orbit. Illumination level on the ground and the required control effort were discussed for a reflector deployed from the ISS orbit, considering a range of reflector dimensions. The maximum energy delivered to a ground farm is about 10 kW h for a LightSail-type reflector, but it can be increased by an order of magnitude if the reflector size is increased to 20 m. It is shown that for reflector sizes up to 25 meter, standard off-the-shelf CMGs for CubeSats can be used to generate the required control torque for the manoeuvre.

Acknowledgments

This project has received funding from the European Research Council (ERC) under the European Union's Horizon 2020 research and innovation programme (grant agreement No. 883730). CM is also supported by the Royal Academy of Engineering under the Chair in Emerging Technologies scheme.

References

[1] H. Oberth, Methods of space travel, Munich, Oldenburg (1929) 494.

[2] K. A. Ehricke, Space light: space industrial enhancement of the solar option, Acta Astronautica 6 (12) (1979) 1515–1633. doi:10.1016/0094-5765(79)90003-1.

[3] J. E. Canady, J. L. Allen, Illumination from space with orbiting solar-reflector spacecraft, Tech. Rep. NASA-TP-2065, NASA (1982).

[4] L. Fraas, Space mirror orbit for municipal street lighting, in: 70st International Astronautical Congress (IAC 2019), IAF, Washington, DC, USA, 2019, paper no. IAC-19,C3,1,5,x49543.

[5] O. Çelik, A. Viale, T. Oderinwale, L. Sulbhewar, C. R. McInnes, Enhancing terrestrial solar power using orbiting solar reflectors, Acta Astronautica 195 (2022) 276–286. doi:10.1016/j.actaastro.2022.03.015.

[6] O. Çelik, C. R. McInnes, An analytical model for solar energy reflected from space with selected applications, Advances in Space Research 69 (1) (2022) 647–663. doi:10.1016/j.asr.2021.10.033.

[7] T. Oderinwale, C. R. McInnes, Enhancing solar energy generation and usage: Orbiting solar reflectors as alternative to energy storage, Applied Energy 317 (2022) 119154.

[8] A. Viale, O. Çelik, T. Oderinwale, L. Sulbhewar, C. R. McInnes, A reference architecture for orbiting solar reflectors to enhance terrestrial solar power plant output, Advances in Space Research (submitted).

[9] A. Viale, C. R. McInnes, Attitude control actuator scaling laws for orbiting solar reflectors, Advances in Space Research (under review) (2022).

[10] M. M. Mikulas, T. J. Collins, W. Doggett, J. Dorsey, J. Watson, Truss performance and packaging metrics, in: AIP Conference Proceedings, Vol. 813, American Institute of Physics, 2006, pp. 1000–1009.

[11] E. Popov, T. Balan, Engineering mechanics of solids, 1999.

[12] T. Prater, N. Werkheiser, F. Ledbetter, D. Timucin, K. Wheeler, M. Snyder, 3d printing in zero g technology demonstration mission: complete experimental results and summary of related material modeling efforts, The International Journal of Advanced Manufacturing Technology 101 (1) (2019) 391–417.

[13] A. Aboobaker, P. Ade, D. Araujo, F. Aubin, C. Baccigalupi, C. Bao, D. Chapman, J. Didier, M. Dobbs, W. Grainger, et al., The ebex balloon-borne experiment—gondola, attitude control, and control software, The Astrophysical Journal Supplement Series 239 (1) (2018) 9.

[14] A. Kinnaird, Bexus user manual (2014). URL https://eduspace.energia.mta.hu/files/bx_ref_bx_user%20manual%20v6-10_05feb14.pdf

[15] O. Mori, Y. Tsuda, M. Shida, J. Kawaguchi, Dynamic and static deployment motions of spin type solar sail, in: 18th International Symposium on Space Flight Dynamics, Vol. 548, 2004, p. 117.

[16] E. Secretariat, Space engineering, Tech. rep., Report ECSS-E-HB-32-20 Parts 1A–8A. European Cooperation for Space (1998).

[17] N. Wolff, P. Seefeldt, W. Bauer, C. Fiebig, P. Gerding, K. Parow-Souchon, A. Pongs, M. Reiffenrath, T. Ziemann, Alternative application of solar sail technology, in: Advances in Solar Sailing, Springer, 2014, pp. 351–365. doi:https://doi.org/10.1007/978-3-642-34907-2_23.

[18] J. Storch, Aerodynamic disturbances on spacecraft in free-molecular flow, Tech. rep. (2002).

[19] K. Schuettauf, R. Kirchhartz, et al., Rexus user manual (2017).

[20] B. Betts, B. Nye, J. Vaughn, E. Greeson, R. Chute, D. A. Spencer, R. W. Ridenoure, R. Munakata, S. D. Wong, A. Diaz, et al., Lightsail 1 mission results and public outreach strategies, in: 4th International Symposium on Solar Sailing, Kyoto, Japan, 2017.

[21] H. Schaub, J. L. Junkins, Analytical mechanics of space systems, American Institute of Aeronautics and Astronautics, 2009.

[22] Y. P. Semenov, V. Branets, Y. I. Grigor'ev, N. Zelenshchikov, V. Koshelev, A space experiment on unfolding of a filmlike frameless reflector with d= 20 m (znamya-2), Kosmicheskie Issledovaniya 32 (4) (1994) 186–193.

[23] C. Garner, B. Diedrich, M. Leipold, A summary fo solar sail technology developments and proposed demonstration missions, Tech. Rep. JPC-99-2697, NASA (1999).

[24] A. Gaude, V. Lappas, Design and structural analysis of a control moment gyroscope (cmg) actuator for cubesats, Aerospace 7 (5) (2020) 55.

[25] C. Underwood, A. Viquerat, M. Schenk, B. Taylor, C. Massimiani, R. Duke, B. Stewart, S. Fellowes, C. Bridges, G. Aglietti, et al., Inflatesail de-orbit flight demonstration results and follow-on drag-sail applications, Acta Astronautica 162 (2019) 344–358. doi:10.1016/j.actaastro.2019.05.054.

[26] Esa user guide to low gravity platforms.
URL http://wsn.spaceflight.esa.int/docs/EUG2LGPr3/EUG2LGPr3-6-SoundingRockets.pdf

[27] F.-N. C. , Space based solar power - frazer-nash consultancy.
URL https://www.fnc.co.uk/media/e15ing0q/frazer-nash-sbsp-executive-summary-final.pdf